RSC Advances

ROYAL SOCIETY OF CHEMISTRY

www.rsc.org/advances

Thermosensitive Mixed Shell Polymeric Micelles Decorated with Gold Nanoparticles at the Outmost Surface: Tunable Surface Plasmon Resonance and Enhanced Catalytic Properties with Excellent Colloidal Stability

Tao Yin, Xue Liu, Jianzu Wang, Yingli An, Zhenkun Zhang, Linqi Shi**

Key Laboratory of Functional Polymer Materials of Ministry of Education, Institute of Polymer Chemistry, College of Chemistry and Collaborative Innovation Center of Chemical Science and Engineering (Tianjin), Nankai University, Tianjin, 300071, China

E-mail: zkzhang@nankai.edu.cn, shilinqi@nankai.edu.cn

KEYWORDS: gold nanoparticle • mixed shell polymeric micelle • surface plasmon resonance • colloidal stability •catalysis

Abstract

Hybrid particular composites consisting of noble metal nanoparticles (NPs) and polymeric particles have attracted intensive interest, due to the possibility to combine the precious optical and catalytic properties of the former with the stimuli responsiveness and biocompatibility of the latter. However, it is challenging to prepare hybrid particles that simultaneously have tunable optical, catalytic properties and excellent colloidal stability. In the current work, we reported a strategy for such kind of hybrid particles, through covalently decorating the outmost surface of mixed shell polymeric micelles (MSPMs) with gold NPs. For this, two block polymers, poly(ε-caprolactone)-*block*-(ethylene glycol) (PCL-*b*-PEG) and poly(ε-caprolactone)-*block*-poly(*N*-isopropylacrylamide) (PCL-*b*-PNIPAM), were prepared by ring-opening polymerization and reversible addition fragmentation chain transfer (RAFT) polymerization, respectively. Co-self-assembly of the two block polymers result in MSPMs with a PCL core and a mixed shell consisting of PEG and PNIPAM. To the end of each PNIPAM chain in the shell, thiol groups are introduced to act as anchors for *in situ* formation of gold NPs. The

number density of the gold NPs are conveniently tuned through varying the relative amount of PEG/PNIPAM in the micellar shell. Reversible shrinking and extension of the PNIPAM chains regulated by temperature can be used to tune the interparticle distance of the gold NPs, while the whole hybrid particles are stabilized by the stretched PEG chains. The hybrid polymeric micelles exhibit thermoresponsive surface plasmon resonance and enhanced catalytic properties as well as excellent colloidal stability.

Introduction

Noble metal nanoparticles (NPs) made of gold, silver, platinum, etc., have been extensively exploited due to their precious optical and catalytic properties and found applications in a wide spectrum of fields such as catalysis, photoelectric devices and biomedicines.[1-6] At the same time, their organic counterparts, mostly polymeric nanoparticles often with a much larger size, have been playing critical roles in manmade nanoscale platforms for drug delivery, bio-imaging and mimics of biological functions.[7-11] Nowadays, preparation of both kinds of nanoparticles, often being pursued separately, has made significant progresses. Especially, in the cases of polymeric NPs based on polymeric micelles, self-assembly of block polymers offers versatile possibilities to fabricate nano-assemblies with rich morphologies and internal architectures.[12-14] Naturally, combining the two kinds of particles together to create hybrid nanoparticles has come into the sight of many researchers.[15-21] In one hand, polymeric NPs has been wisely recruited as templates either for the formation of the metal NPs,[22-26] or for the three dimensional arrangement of preformed metal NPs.[17, 27-30] On the other hand, installing the polymeric NPs with metal NPs can impart novel functional properties into the otherwise inert polymeric materials to realize functional integration. A large library of hybrid NPs has been prepared which have found many novel applications in such fields as heterogeneous catalysis, efficient cancer diagnosis and treatment, etc.[31-37]

In the hybrid NPs consisting of metal and polymeric NPs, the metal NPs can either be loaded into the core,[36, 38, 39] homogenously distribute inside the whole particles,[23, 26] or locate on the peripheral surface of the polymeric particles[16-18, 29]. Hybrid particles in the last case have a core-shell architecture and are especially attractive for several reasons. First of all, the surface exposed metal NPs can be accessed easily by species in the surrounding media which is important for catalysis

and sensing.[25, 29, 40] Furthermore, it is possible to control the inter-particle distances of metal NPs loaded at the outmost surface, which is well known to be related to the electronic and magnetic properties of the nanoparticles.[18, 41, 42] With such goals in mind, stimuli responsive polymeric components such as thermos-responsive poly(*N*-isopropylacrylamide) (PNIPAM), and pH sensitive poly(vinylpyridine) (PVP), have been used as the anchors for the metal NPs.[41-43] Environmental stimuli, such as temperature or pH can be used to induce reversible collapse/swelling of the polymeric components. Accordingly, the spatial position of the loaded metal NPs can also be fine-tuned, resulting in tunable surface plasma resonance (SPR), surface enhanced Raman scattering (SERS) or catalytic behavior.[41-43] In these examples, an often neglected issue is the colloidal stability of the hybrid particles, i.e, the whole hybrid nanoparticles can still keep discretely separated during performing their function under environmental stimuli. Aggregation under working conditions will compromise the performance of the loaded metal NPs. Such situation might occur to the hybrid particles with gold NPs installed onto a temperature or pH responsive polymeric shell.[44, 45] For instance, the collapsed polymeric component such as PNIPAM is hydrophobic which would introduce attraction between the hybrid particles, often resulting in irreversible aggregation.[44] Alternatively, the interparticle distance can be controlled by the density of the metal NPs loaded onto the peripheral surface of the polymeric particles.[29] If the size of the polymeric template is set, increasing the density of metal NPs means decreasing interparticle distance. However, a convenient way to control the density of the metal NPs with certain precision is desperately needed. To our best of knowledge, only few works have realized such goals.

In the current work, we shall decorate mixes shell polymeric micelles (MSPMs) with gold NPs through in situ reduction of a gold precursor, to prepare hybrid polymeric micelles with thermoresponsive SPR and catalytic properties as well as enhanced colloidal stability. MSPMs refer to core-shell micelles with at least two types of polymeric chains in the micellar shell. One of the chains in the micellar shell can be stimuli responsive, which offer an extremely flexible way to fine-tune the surface properties of the polymeric micelles. For the current work, we shall design MSPMs with a poly(ε-caprolactone) (PCL) core and a mixed shell consisting of poly(ethylene glycol) (PEG) and poly(*N*-isopropylacrylamide) (PNIPAM) through co-assembly of poly(ε-caprolactone)-*b*-PEG (PCL-*b*-PEG) and PCL-*b*-PNIPAM (Scheme 1). The end of each

PNIPAM chain at the outmost of the micelles is coupled with a thiol group which is naturally derived from the reduction of the thiocarbonylthio group of the macro chain transfer agent for the reversible addition fragmentation chain transfer (RAFT) polymerization. In situ reduction of a gold precursor can install the outmost surface of such MSPMs with gold NPs which are stabilized by the thiol groups at the end of the PNIPAM chains. Two advantages are unique to the current strategy. First of all, the co-assembly of two kinds of block copolymers offers the flexibility to control the density of the surface thiol groups which are the main anchoring point of the gold particles. In this way, the number density of the loading gold NPs can also be varied. Furthermore, the interparticle distance of the gold NPs can be fine-tuned by heating and cooling to induce the shrinking/extension of the PNIPAM chains, resulting in tunable SPR catalytic properties. Another advantage is that the whole hybrid particles will be stabilized by the stretched PEG chains in the micellar shell, endowing the current system with excellent colloidal stability under working conditions.

Scheme 1. Schematic illustration of the procedure for preparation of the hybrid mixed shell polymeric micelles decorated with gold NPs on their outmost surface.

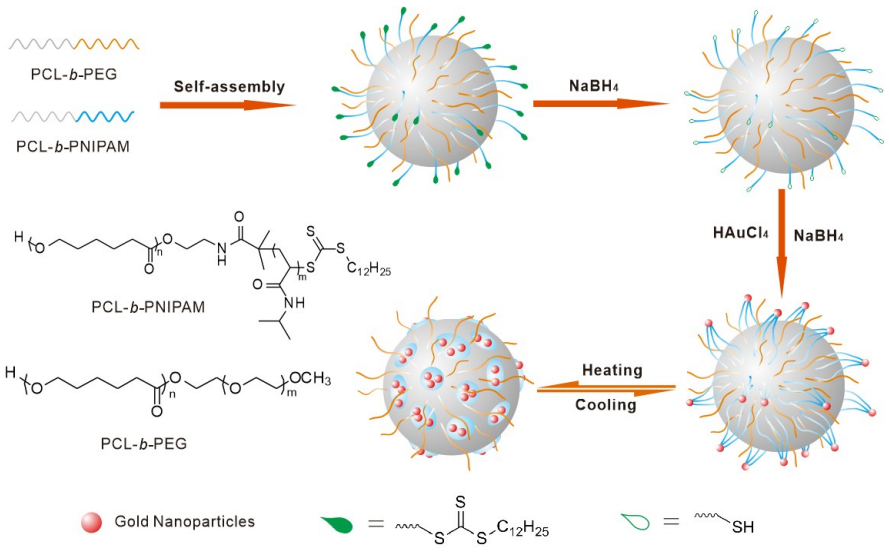

2. Experimental

Materials. $HAuCl_4 \cdot 3H_2O$ (> 99.9%) and NaBH4 (> 98.9%) were obtained from J&K (J&K Scientific Ltd., Beijing, China) and used without further purification. The two block polymers, poly(ε-caprolactone)$_{88}$-*block*-(ethylene glycol)$_{113}$

(PCL_{88}-*b*-PEG_{113}) and poly(ε-caprolactone)$_{83}$-*block*-poly(*N*-isopropylacrylamide)$_{90}$ (PCL_{78}-*b*-$PNIPAM_{90}$), were prepared in our previous work.[46] The subscripts in bock copolymer designate the degrees of polymerization. All the organic solvents were dried following the standard procedure.

Preparation of mixed shell polymeric micelles (MSPMs).

First, 2 mg of the mixture of the two block copolymers, PCL-*b*-PEG and PCL-*b*-PNIPAM with different mass ratios were dissolved in 1.5 mL anhydrous THF. The resulted polymer solution was then added dropwise into 13 mL ultrapure water under vigorous stirring. The solution became opalescent eventually, indicating the formation of micelles. The solution was further stirred overnight and dialyzed against water to remove THF. The final concentration of the micelles was 0.1 mg mL^{-1}. In a similar way, micelles consisting of only PCL-*b*-PNIPAM were also prepared.

Preparation of polymeric micelles decorated with gold NPs.

To prepare hybrid polymeric micelles decorated with gold NPs, the first step is to transform the thiocarbonylthio group at the end of the PNIPAM chains of the micelles into thiol groups. For this, to a 2 mL suspension of the polymeric micelles, 0.5 mL $NaBH_4$ solution (1M) was added. The mixture was stirred for 48 hrs in dark and under nitrogen atmosphere. The final mixture was then dialyzed in a dialysis tube (3.5 kD MWCO, Spectrum) against deoxygenated water under nitrogen atmosphere to avoid oxidation of the thiol groups into disulfide bonds. The dialyzed mixture was concentrated to 2 mL by ultrafiltration centrifugation in an ultrafiltration tube (4k Da MWCO, Millipore) at a centrifuge speed of 4000 rpm. To the suspension maintained at 37 ^{o}C and purged with nitrogen, 400μL aqueous solution of $HAuCl_4 \cdot 4H_2O$ (1.6 mg mL^{-1}) was added under stirring. The mixture was further stirred for another 5 hrs and then 200 μL $NaBH_4$ solution (4 mM) was added. The mixture was stirred for 24 hrs. The final particles were washed by water for three times by centrifuge and redispersion.

Catalytic reduction of *p*-nitrophenol by hybrid polymeric micelles.

The catalytic reduction was carried out in a standard quartz cuvette of 1 cm path length. The aqueous solution of *p*-nitrophenol (350 μL, 0.1 mM) and $NaBH_4$ (150 μL, 10 mM) was mixed

together, the pH of which was kept at 10 by 1 M NaOH solution, if necessary. After the polymeric micelles decorated with gold NPs were introduced to the mixture, the time-dependent absorption spectra were recorded on a TU-8119 UV-vis spectrophotometer. To study the temperature effect, the temperature of the sample holder was controlled with an accuracy of 0.01 ^{o}C by an HAAKE A28 external circulating water bath installed with an HAAKE SC 100 controller (Thermo Scientific). In a similar way, pure gold NPs stabilized by citrate were also assessed.

Characterization.

Transmission electron microscopy (TEM) measurements were performed on a Philips T20ST electron microscope at an acceleration voltage of 100 kV. The TEM samples were negatively stained by uranyl acetate 2% ethanol solution for the bare polymeric micelles while the gold NP decorated ones were directly checked without any pretreatment. Dynamic light scattering (DLS) measurements were conducted on a laser light scattering spectrometer (BI-200SM, Brookhaven) equipped with a digital correlator (BI-9000AT, Brookhaven) at 636 nm at given temperatures. All the samples were obtained by filtering through a 0.45μm Millipore filter. X-ray photoelectron spectroscopy (XPS) measurements were performed with a Kratos Axis Ultra DLD multi-technique X-ray photoelectron spectroscopy (Kratos Analytical Ltd., UK).

Results and discussion

Preparation of mixed shell polymeric micelles.

The two block polymers, PCL_{83}-*b*-$PNIPAM_{90}$ and PCL_{78}-*b*-PEG_{113}, were prepared as reported in our previous publications.[46] Especially, a tailor-designed PCL coupled with a thiocarbonylthio group at one of the chain ends was used as the macro chain transfer agent for reversible addition fragmentation chain transfer (RAFT) polymerization of NIPAM, resulting in PCL-*b*-PNIPAM with the thiocarbonylthio group sitting at the end of the PNIPAM block (Insets of Scheme 1). Following our previous method, co-assembly of PCL-*b*-PNIPAM and PCL-*b*-PEG resulted in mixed shell polymeric micelles (MSPMs) with a PCL core and mixed PEG/PNIPAM shell.[47] The relative ratio of the PEG/PNIPAM in the micellar shell can be adjusted by controlling the relative amount of the two block polymers in the starting materials. The MSPMs were characterized by

dynamic light scattering (DLS) and negative staining TEM (Figure 1). The average hydrodynamic diameter (<D_h>) of the micelles has a typical value of 120 nm and a narrow size distribution at room temperature (Figure 1B). When heating up to more than 32 ^oC, i.e. the lower critical solution temperature (LCST) of the PNIPAM chains, <D_h> decreases to 105 nm while still has a narrow distribution (Figure 1B). As already confirmed in previous works by us and others, at T > LCST, the PNIPAM chains in the micellar shell can collapse from the extended and hydrated state onto the micellar core and form hydrophobic domains while the whole micelles are still colloidally stable due to the steric hindrance offered by the hydrated PEG blocks (Step 4 in Scheme 1).[47, 48] By cooling, the collapsed PNIPAM chains turn into the extended hydrophilic state and the size of the micelles recovered (Figure 1B). In this way, if there are functional species at the end of the PNIPAM chains in the shell, their spatial position in three dimensions is expected to be adjusted conveniently by temperature.[49]

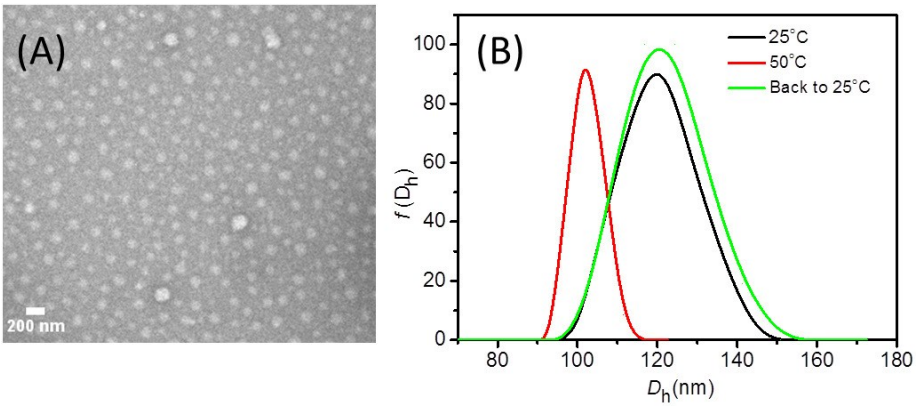

Figure 1. Morphology and size distribution of MSPMs consisting of PCL_{83}-*b*-$PNIPAM_{90}$ and PCL_{78}-*b*-PEG_{113} with a mass ratio 1:9. (A) Photos of the micelles obtained by negative-staining TEM. (B) Hydrodynamic diameter distribution of the micelles revealed by DLS.

In situ formation of gold nanoparticles on the surface of MSPMs.

To decorate the outmost surface of the MSPMs with gold NPs, the thiocarbonylthio end groups at the end of PNIPAM of the MSPMs was first cleaved into thiol groups by the classic $NaBH_4$ reduction (Scheme 1).[45, 50] Into the same mixture in the presence of $NaBH_4$, H_4AuCl_4, the precursor for the gold NPs, was added which was then turned into gold NPs. By optimizing the amount of the precursor relative to the micelle templates, well-dispersed discrete hybrid micelles with gold NPs decorating its outmost surface were obtained which will be referred as

MSPM@AuNP (Figure 2). XPS survey spectra of MSMPs with or without gold NPs indicate that news peak corresponding to Au (4f) appears in the case of MSMPs with gold NPs (Figure S1). In the whole procedure, no external ligand is needed. $NaBH_4$ is a strong reducing agent that leads to a fast rate of nucleation and smaller gold nanopartilces. As soon as gold nanoparticle produced, the surface-exposed thiol groups at the end of PNIPAM in our micelles are chemisorbed onto the surfaces of in situ formed gold nanoparticles, which will stabilize the gold nanoparticles, on one hand. On the other hand, the surface-exposed thiol groups at the end of PNIPAM act as anchor points to limit the location of gold NPs at the micellar surface.[45, 50, 51] Several PNIPAM chains bind to one NP (Scheme 1).[51] The size of the whole hybrid particles has an average size of 130 nm, which is slightly larger than the bare MSPM templates (Figure 3B). The as-prepared hybrid particles can keep colloidal stability under refrigerated conditions for several months without precipitation. Control experiments were performed with similar MSPMs without surface thiol groups and no gold NPs decoration occurred.

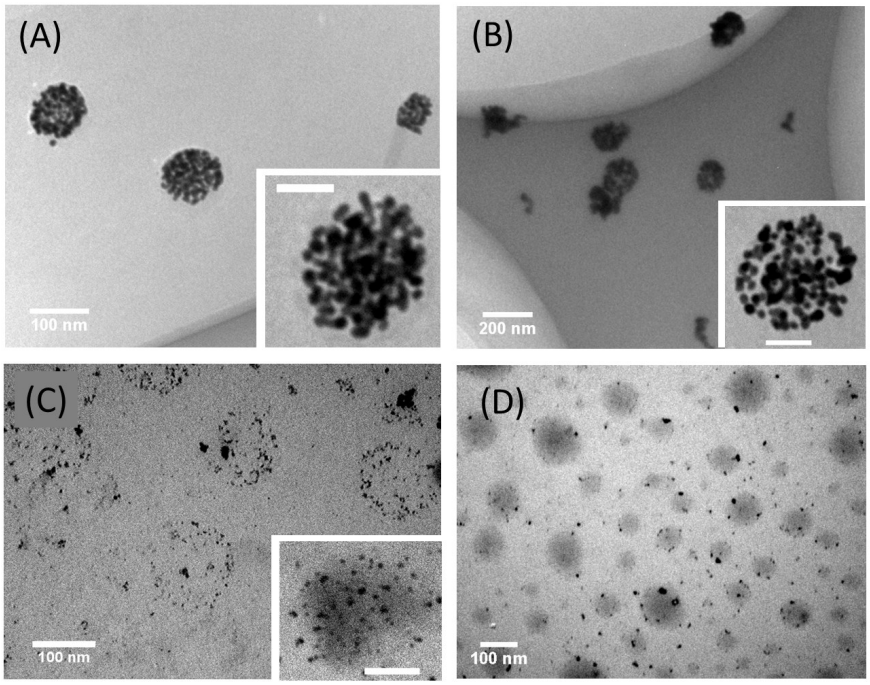

Figure 2. Mixed shell polymeric micelles decorated with gold NPs on the outmost surface. The micelles in (A) is the simple micelle consisting of only PCL-*b*-PNIPAM. The mass ratio of PEG/PNIPAM in the shell of the MSPM in (B), (C) and (D) is 1:9, 1:4 and 1:1, respectively. Scale bar in the insets: 50 nm.

One of the advantages of the current strategy is that the surface thiol groups of the micellar template can be controlled by changing the relative amount of the two block copolymers during self-assembly. By using polymeric micelles with a similar size while various amount of surface thiol groups, the number of the gold NPs on the outmost surface of the MSPM can be fine-tuned (Figure 2). In the case of the simple micelles formed by PCL-*b*-PNIPAM alone, the surface of the micelle has the highest amount of thiol groups. Accordingly, the micelle is decorated with gold NPs which are densely packed (Figure 2A). In the cases of MSPMs, the amount of the thiol in the shell can be reduced by increasing the ratio of PCL-*b*-PEG. The number of the gold NPs on the micellar surface also decreases. For instance, MSPMs with a PEG/PNIPAM mass ratio of 1:9 is still decorated with many gold NPs but increased inter-particle distance and spare spaces are clearly discernable (inset of Figure 2B). After further increasing the PEG/PNIPAM ratio to 1:4, the micelles are only sparsely decorated with gold NPs (Figure 2C). In the case of micelles with a PEG/PNIPAM ratio of 1:1, there are only several gold NPs on the surface of the micelles (Figure 2D). Therefore, the current strategy offers a very convenient way to control the density of the gold NPs on the surface of the hybrid polymeric particles.

The morphology of gold NPs exhibits some unique characteristics which is dependent on the density of the gold particles and is also different from the usual spherical shape of gold NPs obtained in the presence of organic ligands such as citrate (Figure S3A in ESI†). As shown in the insets of Figure 2A and B, many gold NPs have a dumbbell like shape which are probably originated from the fusion of two spherical gold NPs.[52] Discrete spherical gold NPs, with an average diameter of 8 nm become dominant with decreasing thiol groups in the micellar shell (Figure 3C and D).

Thermo-responsive on-particle aggregation behavior of gold NPs without losing colloidal stability of the hybrid micelles.

As discussed before, the terminal functional groups of the PNIPAM chains in the mixed shell of the micelles can change their position with the shrinking and extension of the PNIPAM chains under thermal stimuli. It is therefore expected that the gold NPs at the terminal of the PNIPAM chains can also change their three dimensional position and inter-particle distance reversibly in the similar way. In the case of micelles with a PEG/PNIPAM 1:9, the gold NPs reside at the out most

surface with spare spaces which clearly revealed by TEM (Figure 2B). Upon heating up to LCST, the hybrid particles transformed into a solid-like particles (Figure 3A)，in which the gold NPs densely pack. Although the morphology of the hybrid particles is generally in the spherical shape, their surface becomes rugged (Inset of Figure 3A). The hydrodynamic size distribution from DLS give a sharp peak with a value of 110 nm at T > LCST, lower than 130 nm of the same particle at room temperature (Figure 4B). In addition, the color of the hybrid micellar suspension also changed from the red to deep purple during heating, a clear sign indicating that the surface gold NPs have changed their interparticle distance. These results are both consistent the fact that gold NPs at the terminal of the PNIPAM chains become close to each other with the collapse of the PNIPAM chain during heating. In this way, interparticle distance of gold NPs decreases dramatically, which is beneficial for the optical properties of the particles as will be demonstrated later.

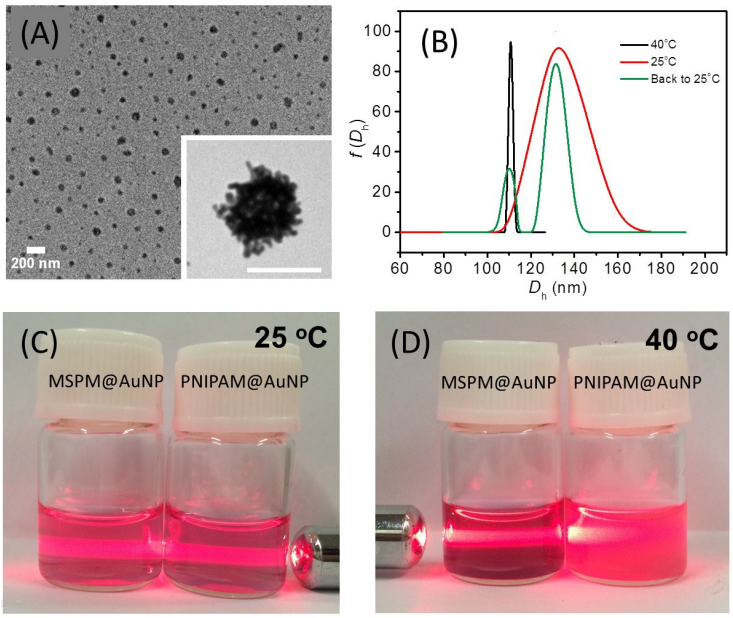

Figure 3. Thermo-responsive behavior of mixed shell polymeric micelles decorated with gold NPs (MSPM@AuNP). (A) TEM photo of MSPM@AuNP after being heated up to 40 ^{o}C and incubated for 30 mins. The PEG/PNIPAM mass ratio of the micelles is 1:9. Scale bar of the inset: 100 nm. (B) Hydrodynamic size distribution of MSPM@AuNP from DLS during heating and cooling. (C) and (D) Tyndall effect of polymeric micelles decorated with gold NPs at room temperature (C) and 40 ^{o}C (D). MSPM@AuNP refers to hybrid particles of (A). PNIPAM@AuNP is based on the simple micelles consisting of only PNIPAM.

The narrow hydrodynamic size distribution at 40 ^{o}C in Figure 3B also indicates that during heating, no aggregation among the hybrid particles occurs. This fact points to the excellent colloidal stability of the hybrid particles based on the MSMPs due to steric hindrance of the stretched PEG chains. This can be also confirmed from visual inspection of the hybrid particle suspension (Figure 3C and D). Pronounced Tyndall effects exist for the hybrid micelles particles either at room temperature or when T > LCST (MSPM@AuNP in Figure 3C and D). However, large aggregates form during heating the suspension of the hybrid micelle consisting of only PNIPAM and gold NPs (Figure S2A in ESI †), which diminish the Tyndall effect (PNIPAM@AuNP in Figure 3C and D).

Listed in Figure 3B is also the hydrodynamic size distribution of MSPM@AuNP after cooling from the heated state back to room temperature, which reveals that the cooled hybrid particles has an average hydrodynamic size matching the value of the same particles before heating. TEM investigation of the hybrid particles cooling back to room temperature also reveals that most of particles can reverse to the state with spare spaces between gold NPs (Figure S2B in ESI†). These phenomena suggest that it is possible to fine tune the three dimensional arrangement and inter-particle distance of the outmost gold NPs by controlling the extension and collapse of the PNIPAM chains. A small population of particles, however, stays in the collapsed state as indicated by the shoulder peak with a maximum value similar to that of the collapsed particles (Figure 3B). This is probably due to the inter particle fusion upon heating, during which neighboring gold NPs permanently stick together.[52, 53] These collapsed hybrid particles also exist in the TEM photos (Figure S2B).

Tunable surface plasmon resonance properties of gold NPs decorated mixed micelles.

One of the prestigious properties of noble metal NPs, including gold NPs, is their surface plasmon resonance (SPR) which has been exploited in many applications. Experimental and theoretical studies have confirmed that such property critically depends on the shape, composition, morphology, and dielectric environment of particels.[35, 36]. In recent years, the focus has been directed to arranging metal NPs into ordered suprastructure with or without templates, which can be used to tune the collective SPR properties of the metal NPs. [29, 36, 54] In these latter cases, it is also demonstrated that the interparticle distance and localized refractive index play critical roles

for a responsive SPR properties. With the current strategy, we have two ways to tune the inter-particle distance of the templated gold NPs and therefore their SPR properties. First of all, the number density of the gold NPs on the outmost surface of the polymeric micelles can be controlled by varying the thiol groups on the surface of the polymeric micelles (Figure 2). The UV-vis absorption spectra of the four kinds of hybrid particles in Figure 2 are presented in Figure 4A, together with citrate stabilized pure gold NPs. By increasing the number density of the gold NPs, i.e decreasing the inter-particle distance, red shift is observed (Figure 4A). The absorption peak shifts from 520 nm of the pure gold NPs to 550 nm of the ones templated on the simple micelles consisting of PNIPAM alone which has the highest density of gold NPs (Figure 2A). Therefore, co-self-assembly of PCL-*b*-PEG and PCL-*b*-PNIPAM into MSPMs is a versatile way to control the number density of the templated gold NPs, resulting in hybrid particles with tunable SPR properties.

Besides the above method, we have demonstrated the reversible packing of gold NPs at the outmost surface of the micelles due to thermo-responsive collapse/extension of the PNIPAM chains. Such tunable spatial reconfiguration is naturally expected to influence the SPR property of the templated Au NPs. Summarized in Figure 4B is the UV-vis absorption spectra of the hybrid MSPM@AuNP with a PEG/PNIPAM mass ratio 1:9 upon heating from room temperature to 40 ^{o}C. Red shift occurs to the absorption peak during heating, and at ca. 32 ^{o}C, the shift levels off (Figure 4C). In this procedure, there is ca 20 nm red shift, from 536 to 556 nm. Furthermore, the absorption spectra also broaden during heating. The turning point at 32 ^{o}C is coincident with the LCST of PNIPAM chains in the shell at which the PNIPAM chains will collapse. Pure gold NPs stabilized by citrate exhibits no such temperature dependent behavior (Figure S3 in ESI†). Therefore, the red-shift and broadening of the UV-vis spectra at T > 32^{o}C should be due to particle-particle coupling effect induced by the on-particle aggregation of the templated gold NPs when the collapse of PNIPAM chains reduces inter-particle distances of the gold NPs. Upon cooling, the absorption peaks recover (Figure 4C). It is noticed that pronounced hysteresis occurs during cooling (Figure 4C). The heating/cooling cycles can be performed for several rounds (Figure 4D). At later stage of the cycles, the absorption peaks after cooling back gradually increase and the degree of red-shift decreases (Figure 4D). As also indicated by DLS in Figure 3B, some hybrid particles stay in the collapsed state after cooling back to room temperature. It is

reckoned that neighboring gold NPs might fuse together when being brought to close with each other during heating since the gold NPs are only stabilized by the end –SH groups of the PNIPAM chains. Similar inter-particle fusion phenomena are also suggested by others.[52, 53]

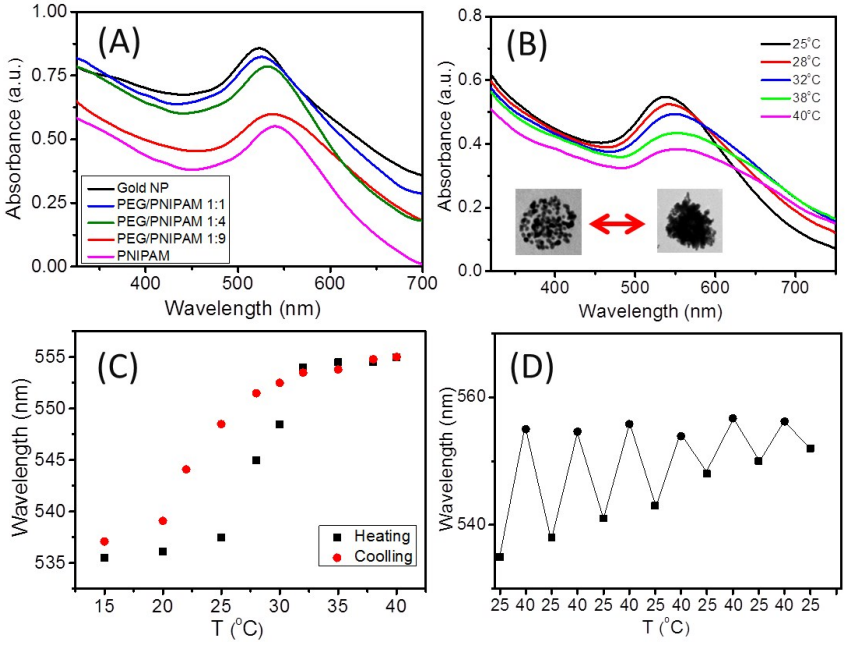

Figure 4. Surface plasmon resonance (SPR) of gold NPs templated by the mixed shell polymeric micelles. (A) UV-vis absorption spectra of the four kinds of hybrid particles in Figure 2 as well as gold NPs stabilized by citrate. (B) UV-vis absorption spectra of the MSPM@Gold NP during heating. (C) The absorption peak versus temperature of the MSPM@Gold NP during heating/cooling. (D) Red shift behavior of the SPR of the MSPM@Gold NP during heating/cooling cycles. The MSPM@Gold NP in (B), (C) and (D) is the same as that in Figure 2B.

Thermal responsive catalytic behavior gold NPs templated by MSPMs.

In order to demonstrate the potential of the current templated gold NPs as heterogeneous catalysts, the catalytic activity of the hybrid micelles was investigated by classic borohydride reduction of *p*-nitrophenol (*p*-NP) to *p*-aminophenol (*p*-AP).[55] It is well established that noble metal nanoparticles can catalyze this reaction and the reaction kinetics can be conveniently monitored by spectroscopic measurements.[31] In the *p*-NP solution under a neutral or acidic condition, a strong absorption peak due to *p*-NP occurs at 317 nm. The peak shifts to 400 nm due to 4-nitrophenolate ions which become dominant when $NaBH_4$ is added to increase the alkalinity of the solution.[59,60] The polymeric micelles decorated with gold NPs were then added to the system and the adsorption

spectroscopy was monitored. The peak at 400 nm decreases and approaches constant during 8 mins, while a new peak at 300 nm appears due to the formation of *p*-AP (Figure 5a and S4 in ESI †). There exists a clear isosbestic point between the two absorption bands in the UV spectra. Therefore, the current hybrid micelles have excellent catalytic properties. This is normally attributed to the decreased size of the gold NPs which corresponds to increasing specific area available to the reduction reaction. It is noted here that our system can keep colloidal stable under the high ionic strength due to the reduction agent of $NaBH_4$, which is sometimes problematic for other supported gold NP system.

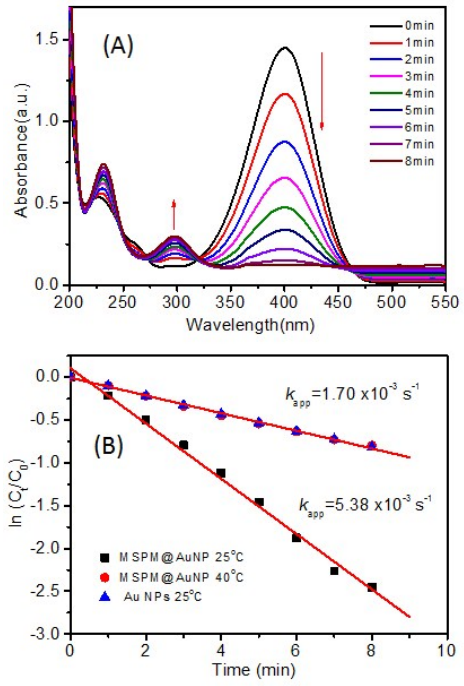

Figure 5. Catalytic behavior gold NPs templated by MSPMs. (A) UV-vis absorption spectra during the reduction of *p*-NP catalyzed by MSPM@AuNP. (B) Plot of $\ln(C_t/C_0)$ versus time during the the reduction of *p*-NP catalyzed by either the citrate acid stabilized gold NP or MSPM@AuNP at varied temperature. The MSPM@AuNP is the same hybrid particles as those in Figure 3.

The kinetics of reduction was determined by measuring the concentrations of *p*-nitrophenolate by recording the absorbance at 400 nm (Figure 5B). The changes of absorbance with time are straight lines, indicating that the reduction reaction follows the first-order kinetics (Figure 5B). The apparent rate constants (k_{app}) of the catalytic reaction at the 25 ^{o}C was estimated by 5.38×10^{-3} s^{-1} for MSMP@AuNP with a PEG/PNIPAM mass ration of 1:9, while 1.70×10^{-3} s^{-1} is estimated for

the pure gold NPs. The three times higher efficiency of the former than the latter can be ascribed to the increasing specific area of gold NPs at the outmost surface of the micelles. To investigate the influence of temperature on the catalytic behavior of the hybrid micelles, the kinetics of reduction of *p*-NP catalyzed by MSPM@AuNP at 40 ^{o}C was also determined, resulting in k_{app} of 1.70×10^{-3} s^{-1} which is nearly identical to the pure gold NPs (Figure 5B). As shown in Figure 3A, the gold NPs of MSMP@AuNP turn into solid-like particles with rugged surface due to the collapse of the PNIPAM chains upon heating. Therefore the whole particles might act like the pure gold NPs.

Conclusions

In summary, a strategy has been devised to prepare hybrid gold/polymeric NPs using mixed shell polymeric micelles (MSPMs) as the template through in situ reduction of gold precursor. Co-assembly of poly(ε-caprolactone)-*b*-PEG (PCL-*b*-PEG) and PCL-*b*-PNIPAM, resulting in MSPMs with a PLC core and a mixed PEG/PNIPAM shell. Thio groups, which are naturally derived from the reduction of the thiocarbonylthio group of the macro chain transfer agent for the reversible addition fragmentation chain transfer polymerization (RAFT), are introduced to the end of the PNIPAM chains. In situ reduction of gold precursor in the presence of such MSPMs produce well-dispersed hybrid particles with their outmost surface decorated with gold NPs, which are stabilized by the thiol groups at the end of the PNIPAM chains. The density of the surface thiol groups and therefore the number density of the gold NPs can be tuned by varying the relative mass ratio of the two block polymers, resulting in hybrid particles with different surface plasma resonance (SPR) properties. Furthermore, the interparticle distance of the gold NPs can be fine-tuned by heating and cooling to induce the shrinking/extension of the PNIPAM chains, resulting in tunable SPR and catalytic properties. The whole hybrid particles are stabilized by the stretched PEG chains in the micellar shell, endowing the current system with excellent colloidal stability under working conditions.

ACKNOWLEDGMENTS

This work was supported by the National Natural Science Foundation of China (No. 21274067, 91127045, 51390483, 51403093), the Fundamental Research Funds for the Central Universities, Natural Science Foundation of Tianjin, China (No. 12JCQNJC01800) and PCSIRT (IRT1257).

† Electronic Supplementary Information (ESI) available: XPS, TEM photos of gold NP decorated polymeric micelles of PNIPAM or MSPMs of a PEG/PNIPAM mass ratio 1:9 after heating, UV-vis absorption spectra during the reduction of 4-NP catalyzed by pure gold NP or MSPM@AuNP after heating, See DOI: 10.1039/b000000x/.

Notes and references

1. J. N. Schrauben, R. Hayoun, C. N. Valdez, M. Braten, L. Fridley and J. M. Mayer, *Science*, 2012, **336**, 1298-1301.
2. H. A. Atwater and A. Polman, *Nat. Mater.*, 2010, **9**, 205-213.
3. S. Eustis and M. A. El-Sayed, *Chem. Soc. Rev.*, 2006, **35**, 209-217.
4. O. V. Salata, *Journal of nanobiotechnology*, 2004, **2**, 3.
5. H. Otsuka, Y. Nagasaki and K. Kataoka, *Adv. Drug Delivery Rev.*, 2012, **64**, 246-255.
6. F. Kretschmer, S. Mühlig, S. Hoeppener, A. Winter, M. D. Hager, C. Rockstuhl, T. Pertsch and U. S. Schubert, *Particle & Particle Systems Characterization*, 2014, **31**, 721-744.
7. J. Panyam and V. Labhasetwar, *Adv. Drug Delivery Rev.*, 2003, **55**, 329-347.
8. J. P. Rao and K. E. Geckeler, *Prog. Polym. Sci.*, 2011, **36**, 887-913.
9. M. Elsabahy and K. L. Wooley, *Chem. Soc. Rev.*, 2012, **41**, 2545-2561.
10. N. Rapoport, *Prog. Polym. Sci.*, 2007, **32**, 962-990.
11. H. Cabral, Y. Matsumoto, K. Mizuno, Q. Chen, M. Murakami, M. Kimura, Y. Terada, M. Kano, K. Miyazono and M. Uesaka, *Nat. Nanotechnol.*, 2011, **6**, 815-823.
12. Y. Mai and A. Eisenberg, *Chem. Soc. Rev.*, 2012, **41**, 5969-5985.
13. H. Qiu, Z. M. Hudson, M. A. Winnik and I. Manners, *Science*, 2015, **347**, 1329-1332.
14. Z. Zhang, R. Ma and L. Shi, *Acc. Chem. Res.*, 2014, **47**, 1426-1437.
15. B. M. Quinn, C. Dekker and S. G. Lemay, *J. Am. Chem. Soc.*, 2005, **127**, 6146-6147.
16. X. Sun and Y. Li, *Angew. Chem., Int. Ed.*, 2004, **43**, 597-601.
17. T. Wu, Q. Zhang, J. Hu, G. Zhang and S. Liu, *J. Mater. Chem.*, 2012, **22**, 5155-5163.
18. H. Xu, J. Xu, X. Jiang, Z. Zhu, J. Rao, J. Yin, T. Wu, H. Liu and S. Liu, *Chem. Mater.*, 2007, **19**, 2489-2494.
19. J. Ou, C. Chang, Y. Sung, K. Ou, C. Tseng, H. Ling and M. Ger, *Colloids and Surfaces A: Physicochemical and Engineering Aspects*, 2007, **305**, 36-41.

20. J. He, Y. Liu, T. Babu, Z. Wei and Z. Nie, *J. Am. Chem. Soc.*, 2012, **134**, 11342-11345.
21. J. Liu, S. Fu, B. Yuan, Y. Li and Z. Deng, *J. Am. Chem. Soc.*, 2010, **132**, 7279-7281.
22. X. Lian, J. Jin, J. Tian and H. Zhao, *ACS Appl. Mater. Interfaces*, 2010, **2**, 2261-2268.
23. R. Liang, J. Xu, W. Li, Y. Liao, K. Wang, J. You, J. Zhu and W. Jiang, *Macromolecules*, 2014.
24. T. Matsushita, Y. Fukumoto, T. Kawakami, T. Tsuruoka, T. Murashima, T. Yanagishita, H. Masuda, H. Nawafune and K. Akamatsu, *RSC Advances*, 2013, **3**, 16243-16246.
25. J. Han, Y. Liu and R. Guo, *Adv. Funct. Mater.*, 2009, **19**, 1112-1117.
26. J. Zhang, S. Xu and E. Kumacheva, *J. Am. Chem. Soc.*, 2004, **126**, 7908-7914.
27. M. Karg, I. Pastoriza‐Santos, J. Pérez‐Juste, T. Hellweg and L. M. Liz‐Marzán, *Small*, 2007, **3**, 1222-1229.
28. A. C. Manikas, G. Romeo, A. Papa and P. A. Netti, *Langmuir*, 2014, **30**, 3869-3875.
29. M. Xie, L. Ding, Z. You, D. Gao, G. Yang and H. Han, *J. Mater. Chem.*, 2012, **22**, 14108-14118.
30. R. A. McMillan, C. D. Paavola, J. Howard, S. L. Chan, N. J. Zaluzec and J. D. Trent, *Nat. Mater.*, 2002, **1**, 247-252.
31. X. Chen, D. Zhao, Y. An, Y. Zhang, J. Cheng, B. Wang and L. Shi, *J. Colloid Interface Sci.*, 2008, **322**, 414-420.
32. J. Hu, T. Wu, G. Zhang and S. Liu, *J. Am. Chem. Soc.*, 2012, **134**, 7624-7627.
33. J. He, X. Huang, Y.-C. Li, Y. Liu, T. Babu, M. A. Aronova, S. Wang, Z. Lu, X. Chen and Z. Nie, *J. Am. Chem. Soc.*, 2013, **135**, 7974-7984.
34. A. K. Gupta and M. Gupta, *Biomaterials*, 2005, **26**, 3995-4021.
35. J. Du, C. Yu, D. Pan, J. Li, W. Chen, M. Yan, T. Segura and Y. Lu, *J. Am. Chem. Soc.*, 2010, **132**, 12780-12781.
36. D. Li, Q. He and J. Li, *Adv. Colloid Interface Sci.*, 2009, **149**, 28-38.
37. J. Li, J. Liang, W. Wu, S. Zhang, K. Zhang and H. Zhou, *New J. Chem.*, 2014, **38**, 2508-2513.
38. R. Contreras‐Cáceres, A. Sánchez‐Iglesias, M. Karg, I. Pastoriza‐Santos, J. Pérez‐Juste, J. Pacifico, T. Hellweg, A. Fernández‐Barbero and L. M. Liz‐Marzán, *Adv. Mater. (Weinheim, Ger.)*, 2008, **20**, 1666-1670.
39. R. A. Álvarez‐Puebla, R. Contreras‐Cáceres, I. Pastoriza‐Santos, J. Pérez‐Juste and L. M. Liz‐Marzán, *Angew. Chem., Int. Ed.*, 2009, **48**, 138-143.
40. S. Wunder, F. Polzer, Y. Lu, Y. Mei and M. Ballauff, *The Journal of Physical Chemistry C*, 2010, **114**, 8814-8820.
41. I. Tokarev and S. Minko, *Soft Matter*, 2012, **8**, 5980-5987.
42. H. Lange, B. H. Juárez, A. Carl, M. Richter, N. G. Bastús, H. Weller, C. Thomsen, R. von Klitzing and A. Knorr, *Langmuir*, 2012, **28**, 8862-8866.
43. Y. Wu, F. Zhou, L. Yang and J. Liu, *Chem. Commun.*, 2013, **49**, 5025-5027.
44. D. Suzuki and H. Kawaguchi, *Langmuir*, 2005, **21**, 8175-8179.
45. M.-Q. Zhu, L.-Q. Wang, G. J. Exarhos and A. D. Li, *J. Am. Chem. Soc.*, 2004, **126**, 2656-2657.
46. X. Liu, Y. Liu, Z. Zhang, F. Huang, Q. Tao, R. Ma, Y. An and L. Shi, *Chemistry-A European Journal*, 2013, **19**, 7437-7442.
47. R. Ma, B. Wang, Y. Xu, Y. An, W. Zhang, G. Li and L. Shi, *Macromol. Rapid Commun.*, 2007, **28**, 1062-1069.
48. S. De Santis, R. Diana Ladogana, M. Diociaiuti and G. Masci, *Macromolecules*, 2010, **43**, 1992-2001.
49. M. Nakayama and T. Okano, *Macromolecules*, 2008, **41**, 504-507.

50. A. B. Lowe, B. S. Sumerlin, M. S. Donovan and C. L. McCormick, *J. Am. Chem. Soc.*, 2002, **124**, 11562-11563.
51. K. H. Bae, S. H. Choi, S. Y. Park, Y. Lee and T. G. Park, *Langmuir*, 2006, **22**, 6380-6384.
52. G. Wang, J. Lian and T.-Y. Zhang, *RSC Advances*, 2013, **3**, 24017-24020.
53. P. Pengo, L. Pasquato and P. Scrimin, *J. Supramol. Chem.*, 2002, **2**, 305-310.
54. X. Shen, C. Song, J. Wang, D. Shi, Z. Wang, N. Liu and B. Ding, *J. Am. Chem. Soc.*, 2011, **134**, 146-149.
55. N. Pradhan, A. Pal and T. Pal, *Langmuir*, 2001, **17**, 1800-1802.